

AUTOMATIC 3D RECONSTRUCTION AND VISUALIZATION OF MICROSCOPIC OBJECTS FROM A MONOSCOPIC MULTIFOCUS IMAGE SEQUENCE

Markus Niederöst^a, Jana Niederöst^a, Jiří Ščučka^b

^a Institute of Geodesy and Photogrammetry, ETH-Hoenggerberg, CH-8093 Zurich, Switzerland, (markus, jana)@geod.baug.ethz.ch

^b Institute of Geonics, Academy of Sciences of the Czech Republic, Studentska 1768, CZ-70800 Ostrava, Czech Republic, scucka@ugn.cas.cz

KEYWORDS: Geomaterials, Multifocus Imagery, Image Processing, 3D Reconstruction, Visualization

ABSTRACT:

Optical microscopy as an important technique in the petrological and mineralogical research enables the observation of highly magnified objects and material structures. However, in case of a non-planar preparation the acquisition of sharp images is - due to the small focus depth of an optical microscope - impossible. The commonly used method to resolve this problem is the acquisition of a sequence of monoscopic images with a constant change of the focal length between consecutive images. The final sharp image is then calculated from this sequence by combining the sharp regions of the raw images. In this paper, we present a simple method to reconstruct the composed image using variance as a criterion for sharpness. As our main focus, we then describe two procedures for generation of textured 3D models from the multifocus image sequence and validate our results. The developed system Shape From Focus is user friendly and Windows-based. It enables fully automated and fast object reconstruction and offers some innovative tools for interactive visualization. The paper also discusses practical aspects of 3D visualization in the study of geomaterials and brings an overview of alternative methods.

1. INTRODUCTION

The generation of high quality microscopic images and 3D models of spatial objects is a task of great concern in the study of geomaterials. Scanning electron microscopy provides a very detailed and sharp 3D representation of the studied object on the computer screen and thus it is a suitable means for reconstructing various mineralogical and petrological samples. However, scanning electron microscopy is very expensive and time-consuming, which prompts many researchers to resort to the much more accessible technique of optical microscopy. The major difficulty associated with using an optical microscope for 3D visualization is its small focus depth that makes the acquisition of sharp images of three-dimensional objects impossible. Thus, to obtain a sharp 2D sample representation as well as to recover its 3D structure, methods of image processing must be applied.

We developed a software system, which combines multifocus optical microscopy and digital image processing for automated generation of interactive textured 3D models. The idea of such a monocular depth recovery goes back to the early eighties. The experimental work of (Pentland, 1982) showed that two images taken with different apertures or with different focal lengths are a source of depth information. In the following years the methods were improved and became more general (Ens et al, 1993, Baba et al, 2002). Surprisingly, these techniques remain rather a computer vision domain; researchers in the application fields such as biology and geology mostly employ stereomicroscopy to obtain 3D views of studied objects (Greenberg et al, 1997). The most recent study of the two- and three-dimensional processing of multifocus images – an approach similar to the one we use – can be found in (Martišek, 2002). As there is a lack of operational software offering a 3D information of optical microscope outputs, we see our main

contribution in providing an easy-to-use system including several innovations in terms of interactive 3D visualization.

In this paper we first explore the possibilities of application of our system in the study of geomaterials and give an overview of alternative methods (Section 2). In Section 3, the generation of a sharp image from a multifocus image sequence is described, followed by the presentation of our methods for recovering depth from microscopic imagery (Section 4). Section 5 brings possibilities of 3D visualization of microscopic samples, followed by an evaluation of our results in Section 6. Finally, we present our software Shape From Focus in Section 7 and end up with conclusions and outlook.

2. 3D VISUALIZATION IN THE STUDY OF GEOMATERIALS

Conventional optical microscopes provide magnified and sharp *two-dimensional* images of *planar* objects. For the microscopic observation in the petrological and mineralogical research, two types of particularly prepared planar sections of the studied material are usually used: so called polished and thin sections (Fig. 1). Such preparations enable the visualization of structure, texture and material composition. Size, shape, orientation and distribution of grains, material failure, proportional representation of individual components and other characteristics can be measured. Using appropriate stereological methods, volume values of measured parameters can be estimated according to the plane measurements, too.

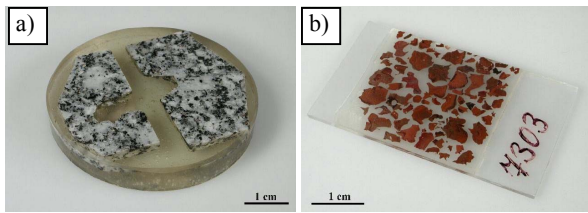


Fig. 1: Standard microscopic preparations: a) Polished section of granite sample with pulsed high-speed water jet cuts, b) Thin section of copper slag grains

However, there exist many geomaterials where the creation of standard microscopic preparations is not possible, because this procedure would cause the distortion or loss of the image information. For example, this is the case of geocomposite materials such as the crushed slate hardened with polyurethane resin (Fig. 2). The epoxy impregnation and grinding of the composite would lead to undesirable effects: the deficient adhesion of the foam material to the rock grains would not be visible anymore. Therefore after cutting the material with a diamond saw no further processing of the preparation is applied. The resulting cut keeps all the necessary image information, however, it is due to missing epoxy impregnation and grinding in fact *non-planar*. In addition to (nearly) planar objects and scenes, it is also necessary to visualize and analyse *spatial* objects such as microcrystals, loose material particles (Fig. 3 and 4), microfossils (Fig. 13), the surface of cut planes after the interaction of cutting tools with disintegrated material, etc.

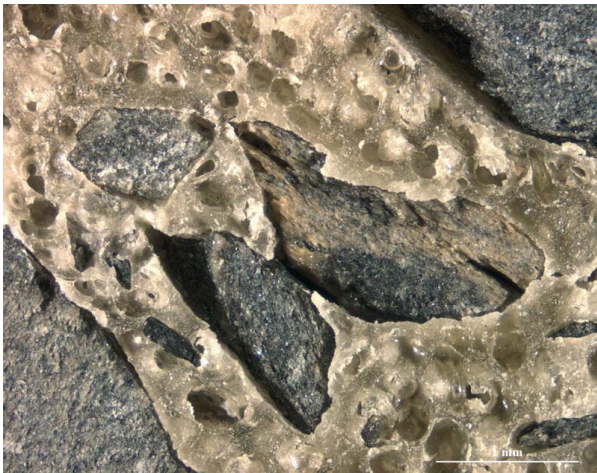


Fig. 2: Texture image of geocomposite material obtained by reconstruction from multifocus image sequence (Section 3). Note the deficient adhesion of the foam material to the rock grains.

Thus, we can see that high quality microscopic images as well as 3D models of *spatial* objects can provide essential information for many applications. To give some more practical aspects of this issue, we shortly discuss the use of 3D visualization in Abrasive Water Jet (AWJ) Technology in the next subsection. In order to understand the advantages and limitations of our system and thus making a better use of it we also categorise existing methods dealing with 3D visualization in the study of geomaterials (Section 2.2).

2.1 3D visualization in the Abrasive water jet technology

Abrasive water jet technology is one of the fields where the methods for 3D visualization play an important role. This modern and constantly developing technology applies the high-speed water jet with the assistance of powered abrasive materials for cutting, disintegration and surface treatment of various materials. In principle, there is no material that could not be cut using this technology (Foldyna, Sitek 2002). Abrasives can be mineral sands (especially garnet and olivine) and various waste materials, e.g. slag. In medical science and food industry, various saccharides and salts are used, too. Properties of used abrasives determine the cutting efficiency of the AWJ system and quality of the disintegration process in a significant way. Therefore it is necessary to study the morphology of abrasive grains – i.e. their shape, size, surface character of individual grains, their deformation and inclusion impurities. The particle shape and size analyses of already used abrasive concentrates are very important for economic reasons as concerns the grain recycling. The study of the interactive process of the water jet with abrasive grain in the mixing chamber or the abrasive water jet interaction with a cut material requires a detailed analysis of grain shape and size, too. The size, shape and failure character of mineral grains released in cutting kerfs of a disintegrated geomaterial are studied together with the abrasive grains.

2.2 Methods for 3D visualization of geomaterials

There are three commonly used methods for visualization of geomaterials nowadays. However, all of them face some drawbacks in terms of applicability and quality of the three-dimensional result. We list the main features of these methods:

1. **Scanning Electron Microscopy (SEM):** The Scanning Electron Microscope creates highly magnified grey scale images of studied objects (Fig. 3). Samples must be carefully prepared to withstand the vacuum inside the microscope and to conduct electricity. This is done by sticking the sample on a special holder and coating it with a thin layer of various metals (gold, silver, copper etc.) or carbon. The electron beam hits the sample surface spot by spot. The emitted secondary electrons are caught by the detector and transformed into a signal that creates an image on the computer screen. The result is a very detailed, complex and interactive 3D sample representation. The drawback of this method is – except of its high costs – a time-consuming preparation of the samples. In addition, it is not possible to visualize orientation and quality of cracks and inclusions inside the studied material. As mentioned in Section 2.1, the latter is essential for the study of mineral abrasive grains in the AWJ technology (compare Fig. 3 and 6).

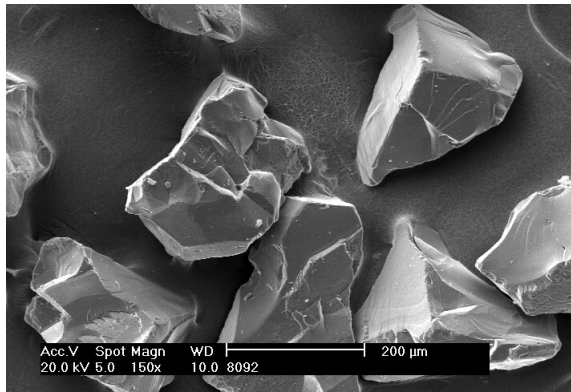


Fig. 3: SEM microphotography of mineral abrasive grains (garnet almandine, SEM Philips XL 30). The character of the grain surface made by fracture plains is well visible on the image.

2. **Stereo Optical Microscopy:** The stereo optical microscope allows viewing and measuring objects in stereo mode. However, this effect is only temporary and cannot be preserved in the same quality outside the microscope. There exist several systems for so called direct-view 3D microscopy using conventional lenses, e.g. a method of multiple oblique sample illumination or a dual oblique viewing. For the latter, a novel 3D head for a microscope replaces the standard trinocular head and converts the 2D image into a 3D image (Greenberg et al, 1997).
3. **Optical Microscopy:** As mentioned before, the small focus depth of an optical microscope causes the effect, that a non-planar sample cannot be displayed sharply in a full extent. Therefore the following procedure of image reconstruction can be applied: A sequence of monoscopic images of the studied object (e.g. grain) is scanned step by step with changing focal length. Then a digital image processing system selects only the sharp fractions, the so called “optical cut”, from every image of the sequence. The final high quality grain image is obtained by the composition of extracted optical cuts (Fig. 4). To generate a spatial model of the object, the depth is estimated according to focussing distance of a particular image of the sequence (Ens et al, 1993, Kaufhold et al, 1998, Baba et al, 2002, Martišek, 2002).

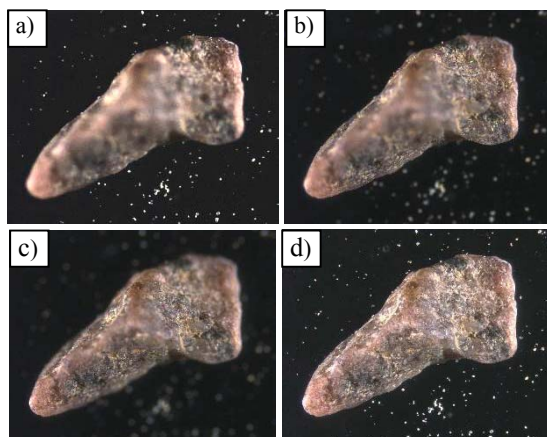


Fig. 4: The procedure of image reconstruction. a)-c) Three of 24 images of a grain of sand taken through an optical microscope with varying focussing distance, d) The composed image.

For practical reasons (availability of an appropriate system), we decided to use the monoscopic optical microscopy in combination with digital image processing. The question is *how* to find the optimal image fractions for the 2D and 3D reconstruction procedure. Most of the existing techniques are based on modeling the optical system’s Point Spread Function and removal of out-of-focus blur. This deconvolution method usually requires a calibration procedure or an object containing clear edges (Kaufhold et al, 1998, Asada et al, 2001). Other methods are semi-automated, such as (Kaufhold et al, 1998). The advantage of our approach to 2D (Section 3) and 3D (Section 4) reconstruction is that almost no pre-knowledge is required and the procedures work fully automatically.

The result of our spatial reconstruction is an interactive textured 3D model of the sample containing information that could not be provided by the optical system of the conventional microscope.

3. MULTIFOCUS IMAGE SEQUENCE AND THE COMPOSED IMAGE

Due to the small focal length of an optical microscope, it is not possible to get a sharp representation of a 3D object with just one image. Therefore a sequence of monoscopic images of the studied object is scanned step by step with a constant change of the focussing distance between consecutive images. The composed image is then calculated from this sequence by combining the sharp regions (optical cuts) of the raw images. In our approach we use local variance as criterion for sharpness (Fig. 5). The result is a focused representation of the complete object.

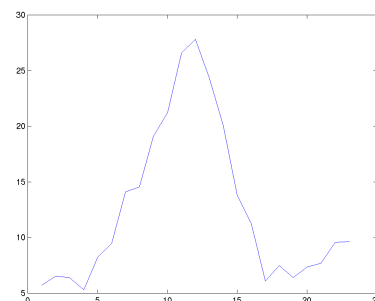


Fig. 5: Variance at coordinates x, y for all 23 raw images. The raw image with the maximum variance contains the sharpest image information at point x, y .

In our system, the color $RGB_{x,y}$ of a pixel at x, y position in the composed image is determined in the following manner: For each of the raw images, the grey value variance of the $n \times n$ neighbourhood at position x, y is calculated. Note that for the variance calculation the color values of the pixels are transformed to grey scale.

$$GV_{xy} = 0.33 \cdot (R_{xy} + G_{xy} + B_{xy}) \quad (1)$$

where

x, y	Image coordinates
GV_{xy}	Grey value at image coordinates x, y
R_{xy}, G_{xy}, B_{xy}	Red, green and blue color of a pixel at x, y

The patchsize $n \times n$ is selected by the user before processing the data. The choice of the patchsize is not critical. Usually the calculations are done with $n = 9$. Variance $v_{xy}(R)$ of raw image R at x, y is then given by

$$v_{xy}(R) = \frac{1}{n^2} \sum_{i=x-k}^{x+k} \sum_{j=y-k}^{y+k} (GV_{ij} - \overline{GV})^2 \quad (2)$$

where

$v_{xy}(R)$	Variance of the R -th raw image at x, y
n	Patchsize
k	$(n-1) / 2$, calculated from the patchsize
x, y	Image coordinates of current pixel
GV_{ij}	Grey value at image coordinates i, j
\overline{GV}	Mean grey value in $n \times n$ current pixel neighbourhood

Now the raw image R_{max} with the highest variance $v_{xy}(R)$ is determined. The color RGB_{xy} in the composed image is taken from the color raw image R_{max} at x, y .

The results of the multifocus image reconstruction are depicted in Fig. 2, 4d and 6. Our procedure is simple: we did not invest to more sophisticated solutions on purpose. The reason was that at the Institute of Geonics Ostrava, which is involved in the geological part of our project, the complex image analysis system LUCIA DI is available. This system, developed by the Czech company Laboratory Imaging Ltd., Prague, supports multifocus image acquisition in combination with an optical microscope, generation of the composed image and offers many other analysis functions. Therefore we rather focused on the topics described in the following, as they are not part of the LUCIA DI software package.

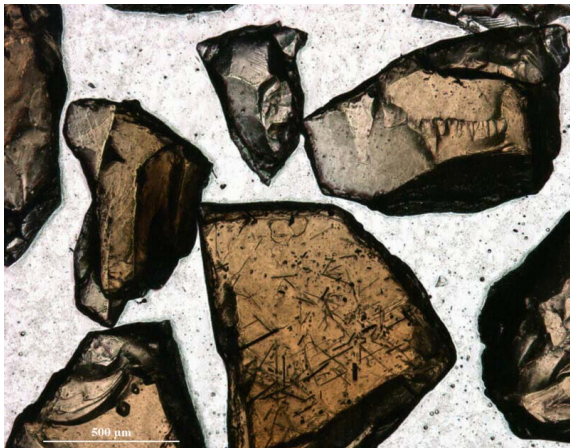


Fig. 6: Reconstructed image of mineral abrasive grains (garnet almandine, optical microscope Olympus BX 50, objective UPlan FI 4x/0,13, transmitted light). The acicular inclusions of mineral rutile are obvious in the big grain in the middle of the image (in opposite to Fig. 3).

4. 3D RECONSTRUCTION USING A MULTIFOCUS IMAGE SEQUENCE

We developed two methods for the 3D object reconstruction from the multifocus image sequence. The first one, which we

call the method with maximum variance, differs only little from our approach for the composition of a sharpened image described in Section 3. The second, more accurate method uses a parable fit to a sample of variances.

4.1 Method with maximum variance

In order to eliminate errors in the background of the reconstructed object, it is necessary to indicate a binary mask that separates the fore and the background of the image data (Fig. 7). For this purpose we propose to make a copy of the composed image. The copy is then edited in a common paint program. The foreground is painted white, the background is painted black.

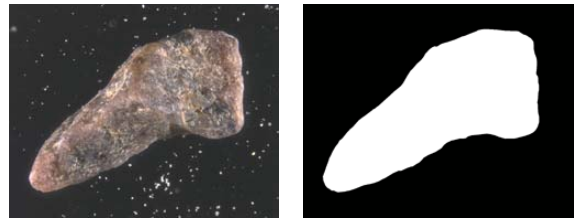


Fig. 7: Composed image and binary mask, which is used to exclude the background from the reconstruction process.

The content of the used raw images is again transformed to grey scale and a patchsize $n \times n$ is selected by the user. The raw images have to be ordered according to the focussing distance and an index i is assigned to each of them. The number of raw images is N . Image 1 is the one with the longest focussing distance, image N the one with the shortest focussing distance.

For data volume optimization in the resulting height model, only each t -th image point is processed. The thin out factor t is user defined and gets usually a value of 4. For each point x, y where x and y are multiples of t , the variance $v_{xy}(R)$ of raw image R at x, y is calculated from Equation 2.

Now the raw image R_{max} with the highest variance $v_{xy}(R)$ is determined. The height of the currently processed point x, y is given by the index $i(R_{max})$ of that particular raw image, multiplied with a height factor.

$$h_{xy} = i(R_{max}) \cdot hf \quad (3)$$

where

h_{xy}	Height of the object at coordinates x, y
$i(R_{max})$	Index of the raw image with highest variance
hf	Height factor

The height factor is used to preserve the correct ratio between the planar extensions and the height of the object. It is calculated from the image dimensions n_x, n_y in pixel, the metric dimensions d_x, d_y of the sensor in microns and the thin out factor t .

The resolution of the image (metric size of one pixel) is calculated as

$$res = \frac{d_x}{n_x} = \frac{d_y}{n_y} \quad (4)$$

where

res	Image resolution in microns
d_x, d_y	Metric image dimensions in microns
n_x, n_y	Image dimensions in pixel

Taking care that a thin out factor t was used for data reduction, the height factor hf is now given by

$$hf = \frac{fds}{res \cdot t} \quad (5)$$

where

hf	Height factor
fds	Focussing distance step between images
t	Thin out factor

The method only allows to calculate a restricted number of N different height values, because the focussing distance was changed in discrete steps. This causes a so-called staircase effect (Fig. 8; mentioned also in Martišek, 2002). In addition the model yet contains some erroneous heights. For postprocessing we use a 5×5 local median filter to remove coarse errors and a 7×7 or 9×9 local average filter to eliminate the staircase effect (Fig. 9).

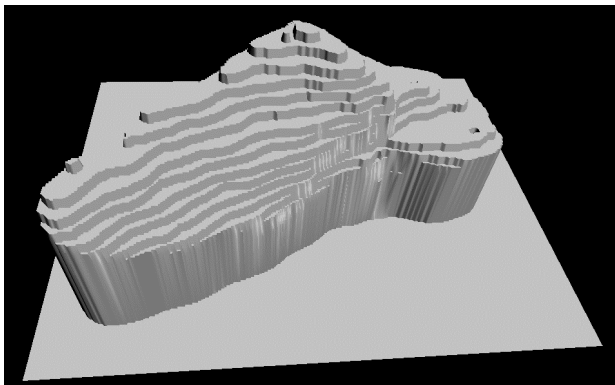


Fig. 8: The staircase effect of the method with the maximum variance (before application of local average).

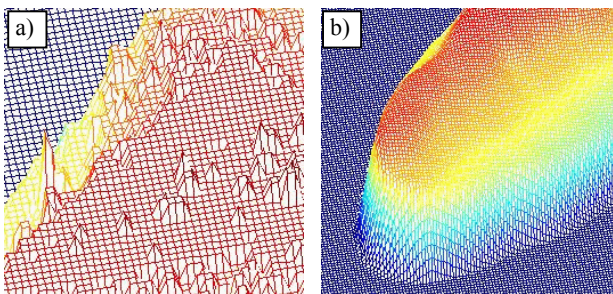


Fig. 9: Reconstruction result as wire frame model. a) Detailed view of outliers before postprocessing, b) The model after postprocessing with local median and local average.

4.2 Method with parable fit to a sample of variances

This approach was developed in order to avoid the restriction that only those height values can be determined that are a multiple of focussing distance step fds .

First the raw image with the maximum variance is determined as described in Section 4.1. Now a parable is optimally fit to the graph of variances, using 7 observation points:

$$v_{xy} = a \cdot h_{xy}^2 + b \cdot h_{xy} + c \quad (6)$$

where

v_{xy}	Varinace of the current raw image at x,y
h_{xy}	Height of the point (or focussing distance, respectively)
a, b, c	Parameters to be estimated

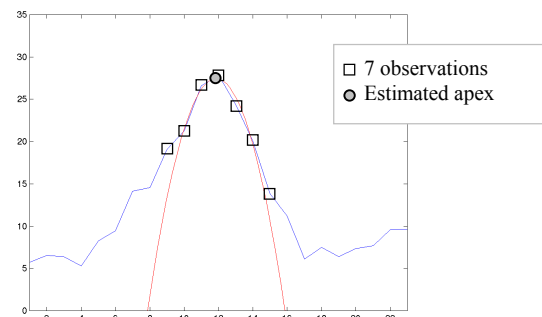


Fig. 10: Graph of grey value variance through a sample of raw images at the same pixel position. The parable is fit to the point with maximum variance and the 3 closest samples on the left and the right side.

The equation system for the least squares fitting can now be formulated with the given 7 points (see Fig. 10). After calculating the unknown parameters, the abscissa value of the apex is calculated with

$$sx = \frac{-b}{2a} \quad (7)$$

where

sx	Abscissa value of the apex
a, b	Estimated parameters of the parable

The x-coordinate sx of the apex is now taken as height value h_{xy} for the resulting height model.

With the use of fitted parables instead of the maximum variance, the heights in the resulting model are no longer restricted to be a multiple of the focussing distance step. Therefore no stairs effect occurs.

Again we used postprocessing with the local median (7×7 neighbourhood). Although there is no stairs effect in the model, the use of a local average (7×7 neighbourhood) leads to a visual improvement of the object representation.

5. VISUALIZATION

The resulting height model is saved in the commonly known VRML2 format (Virtual Reality Modelling Language), where the composed image calculated in Section 3 is used as texture. We take advantage of the new possibilities of VRML2 format: in particular the *ElevationNode* that specifies a uniform rectangular grid in the XY-plane of a local coordinate system. The geometry is described by a scalar array of height values that assigns the height of a surface above each point of the grid. In the header of the node, the X- and Y-spacing as well as the grid width are defined. The *ElevationNode* even enables to project the texture automatically, so that neither triangle vertices nor texture coordinates must be included. In addition, parameterised tiling of both height model and texture is also possible. Obvious advantage of using this specification in a comparison with VRML1-based methods is an extreme reduction of data volumes and improvement of the navigation performance. Surprisingly, there are still many even commercial applications that do not consider this important aspect of visualization and only allow exporting “classical” VRML1-based models.

An example of a VRML model of the reconstructed grain of sand in the freeware Cosmoplayer is depicted in Fig. 11.

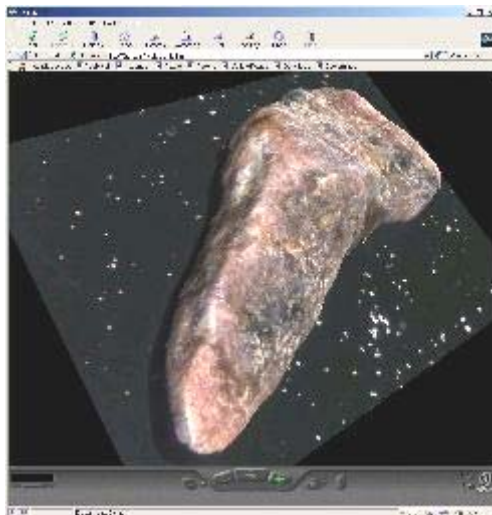


Fig. 11: The reconstructed grain of sand (object size in plane about 4 x 2 mm) in the freeware Cosmoplayer.

We also developed an own 3D viewer, which enables navigation in reconstructed 3D models, generation of videos in AVI format and creation of stereo anaglyph images (Fig. 12 and 13). It is possible to visualize wireframe models, too (Fig. 14).

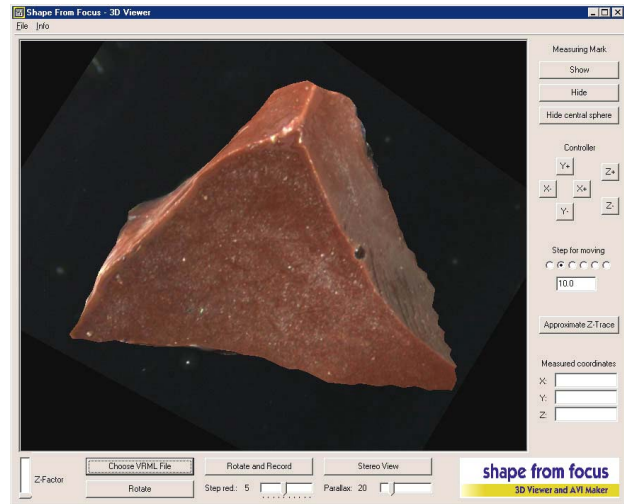


Fig. 12: The reconstructed copper slag (object size in plane about 1.5 x 1.5 mm) in the viewer of our software Shape From Focus.

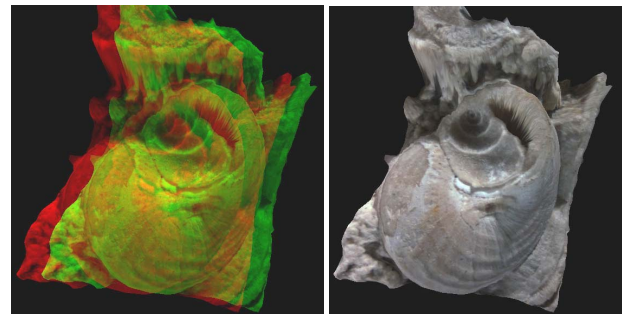


Fig. 13: Stereo anaglyph view of the gastropod fossil (object size in plane about 3 x 4 mm) to be viewed with red/green anaglyph glasses) and its textured representation.

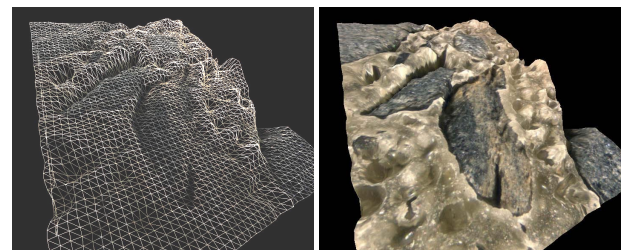


Fig. 14: The 3D model of a crushed slate hardened with polyurethane resin (object size in plane about 3 x 4 mm) as a wire frame and textured representation.

An integrated part of our viewer is a novel tool for measurements in the 3D model. A 3D measuring mark placed onto the model surface enables measurement of 3D coordinates (Fig. 15).

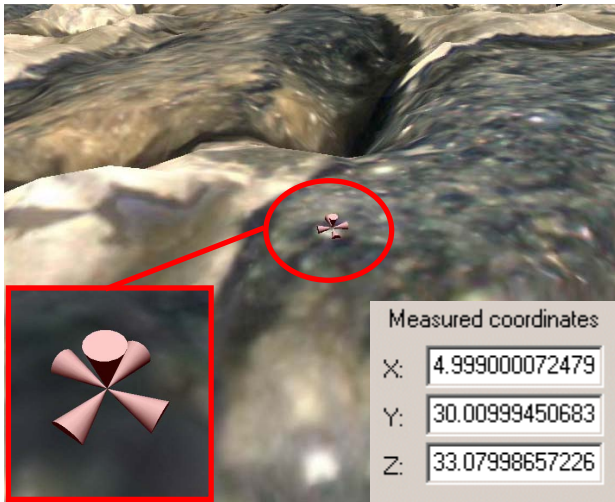


Fig. 15: 3D measuring mark in Shape from Focus.

6. VALIDATION OF RESULTS

For the evaluation of our implemented methods a tilted thin section, i.e. a perfectly planar cut was scanned in a sequence of 20 images with a focussing distance step of 51 microns. The object was reconstructed with both previously described methods, using a 9x9 patch size for the variance (Fig. 16). For the postprocessing a 9x9 median filter was applied, followed by calculation of the local average in a 5x5 neighbourhood.

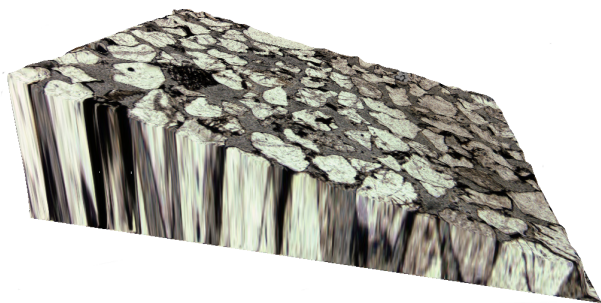


Fig. 16: The 3D model of the test object (tilted thin section of a sandstone) that was used for the estimation of the height accuracy.

Surface profiles of the tilted thin section should be straight lines, so the following method was used to estimate the height error of a reconstructed object: From the 16 created profiles, the standard deviation of a single height was estimated with linear regression (Fig. 17).

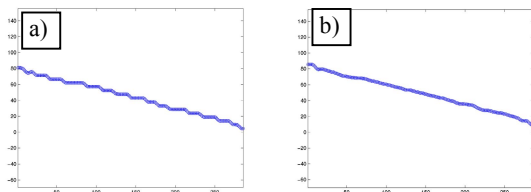


Fig. 17: Profiles of the test object, a) reconstruction from variances with visible stairs effect b) reconstruction with the parable method.

For the method with parable fit to a variance sample, the mean standard deviation from 16 profiles was 9.3 microns. Considering the object size of 4179 x 3297 x 972 microns, the accuracy is not excellent, but certainly sufficient for visualisation purposes.

The accuracy from the method with maximum variance was 12.9 microns. Main reason for the higher standard deviation is the staircase effect caused by the fact that only heights are determined that are multiples of the focussing distance step.

The staircase effect could be reduced by choosing a larger patch size for the local average calculation. This is certainly an appropriate means for visualisation. On the other hand some details might be smoothed out. For the difference image between the two developed reconstruction methods showing the impact of the staircase effect see Fig. 18.

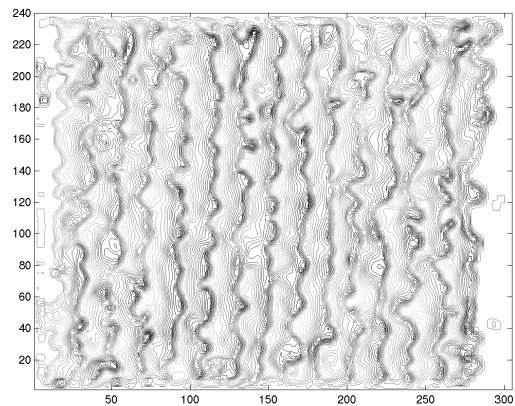


Fig. 18: Contour lines of the difference between the calculation using the variance maximum the parable method.

The accuracy of the results could certainly be improved, if the focussing distance step between two adjacent raw images was reduced. This would result in a larger number of raw images which is not critical due to the fast and automated processing.

7. THE SOFTWARE

The presented algorithms were implemented as a stand-alone software package called Shape From Focus (Fig. 19), running on Microsoft Windows. The module for the calculation of composed images and for the 3D reconstruction was programmed in Borland Delphi 6.0, whereas for the viewer Delphi 6.0 was used in combination with GLScene, an OpenGL based 3D library for Delphi that is distributed under the Mozilla Public License (GLScene, 2003).

Tests were done on a computer with a 1.7 GHz Pentium 4 processor and 512 MB RAM in order to estimate the time for different processing steps. The calculation of the composed image from 23 raw images takes around 1 minute. This gives an average processing time of less than 3 seconds per raw image. The 3D reconstruction with the maximum variance (9x9 patch, thin out factor 4) requires for the same input data about 20 seconds; the parable method is only insignificantly slower. The postprocessing of the resulting 3D model with the local median or the local average is done in a second.

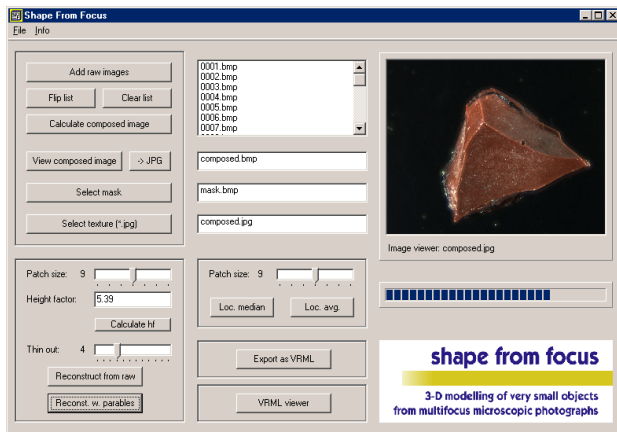


Fig. 19: User interface of our system Shape From Focus.

The numbers above show that even on an older computer and with the manually produced binary mask for the exclusion of the background, it won't take longer than 5 minutes to produce an interactive 3D model or an anaglyph stereo view of a microscopic object from a multifocal image sequence.

8. CONCLUSIONS

Our system 'Shape From Focus' represents an effective way of fully automated reconstruction and 3D visualization of microscopic objects. The combination of optical microscopy and our method is essentially cheaper and less time-consuming than the Scanning Electron Microscopy and it even brings two additional advantages. First, optical microscopy allows the visualization of orientation and quality of cracks and inclusions inside the studied material, what is not possible under the electron microscope. Second, as the optical microscope enables the observation of individual objects in polarised transmitted light, such an image can be used as a texture for the reconstructed model, too.

The main value of our system in opposite to all commonly used procedures is that it can produce interactive, texture-mapped and durable 3D models for visualization purposes. The procedures do not yet work fully automatically – the generation of a binary mask is still done in the manual mode. However, we do not consider the automation of this step by thresholding and application of morphological operators a particular problem and we plan to come up with a respective solution in the future. Our upcoming work will also include implementation of the automated elimination of outliers in the reconstruction procedure using a parable fit. We believe that these improvements will lead to a robust and more accurate system for interactive 3D visualization in the study of geomaterials within a minimal timespan and with very little operator interference.

9. ACKNOWLEDGEMENT

The part of this work done at the Institute of Geonics in Ostrava was financially supported by the Grant Agency of the Academy of Sciences of the Czech Republic, No. A 3086201.

REFERENCES

- Asada, N., Baba, M., Oda, A., 2001. Depth from Blur by Zooming. Proceedings of the Vision Interface Annual Conference, Ottawa, Canada.
- Baba, M., Asada, N., Migita, T., 2002. A Thin Lens Based Camera Model for depth Estimation from Defocus and Translation by Zooming. Proceedings of the 15th International Conference on Vision Interface, Calgary, Canada.
- Ens, J., Lawrence, P., 1993. An Investigation of Methods for Determining Depth from Focus. IEEE Transactions on Pattern Analysis and Machine Intelligence. Vol. 15, No. 2, pp. 97-108.
- Foldyna, J., Sitek, L., 2002. Water Jet Cutting. Proceedings of the workshop Surfacing and Thermal Coatings in Production and Reparation, VSB-TU Ostrava, Czech Republic, pp. 99-106 (in czech).
- GLScene, 2003. GLScene – OpenGL Solution for Delphi. Founded and previously developed by M. Lischke, currently developed and maintained by E. Grange. www.glscene.org, last visited on 20 January 2003.
- Greenberg, G. L., Boyde A., 1997. Direct View 3-D Microscopy Using Conventional Lenses. *European Microscopy and Analysis*, March, pp. 5-7.
- Kaufhold, J., Karl, W. C., 1998. A Nonparametric Defocus-based Approach to Reconstructing Thin 3D Structures in Optical Sectioning Microscopy. Proceedings of the International Conference on Image Processing, Part II, pp. 953-957.
- Martišek, D., 2002. The Two-Dimensional and Three-Dimensional Processing of Images Provided by Conventional Microscopes. *Scanning*, Vol. 24, 284-295, pp. 284-295.
- Pentland, A. P., 1982. Depth of Scene from Depth of Field. Proceedings of the Image Understanding Workshop, pp. 253-259.